J. CHEM. SOC. FARADAY TRANS., 1994, 90(15), 2257–2264

Characterisation of Iron/Titanium Oxide Photocatalysts

Part 2†.—Surface Studies

Roger I. Bickley*
Department of Chemical Engineering/Chemistry and Chemical Technology, University of Bradford, Bradford, West Yorkshire, UK BD7 1DP

Teresita Gonzalez-Carreño
Instituto de Ciencia de Materiales, Consejo Superior de Investigaciones Cientificas, Madrid, Spain

Agustin R. Gonzalez-Elipé and Guillermo Munuera
Departmento de Quimica-Inorganica, Facultad de Quimica, Universidad de Sevilla, Sevilla 41011, Spain

Leonardo Palmisano
Dipartimento di Ingegneria Chimica dei Processi e dei Materiali, Università di Palermo, Viale delle Scienze, 90128 Palermo, Italy

A study of the surfaces of particulate solids, formed by the dispersion of iron(III) ions in various titanium dioxide preparations, has revealed that significant changes occur during the calcination of these materials in air at progressively higher temperatures (T/K $\leqslant$ 1273). In the more dilute systems, containing nominal iron(III) concentrations of 0.5–1.0 atom%, solid solutions in the anatase phase exhibit good degrees of dispersion which are maintained as the phase transformation into rutile progresses at more elevated temperatures (T/K $\geqslant$ 923). With the larger nominal iron concentrations (2 and 5 atom%) X-ray photoelectron (XPS) and diffuse-reflectance (DRS) spectroscopic measurements show that the formation of iron-rich surfaces has commenced already at 773 K through there being a lower limit of solubility of iron in the rutile phase and through the anatase to rutile phase transition becoming detectable at lower temperatures in these solids. The Fe : Ti atomic ratios at the surface with the larger nominal concentrations of iron are consistent with the formation of iron-rich surface phases, α-Fe_2O_3 and Fe_2TiO_5. Inhomogeneities in the distribution of the surface ion species have also been demonstrated by EDX measurements.

The structural character of these solids has been discussed in relation to their photocatalytic activities for the reductive fixation of dinitrogen by water, in which only single-phase systems were found to be active. The inactivity of the multi-phasic solids has been considered in terms of the masking of the active phase by surface layers which create electronic heterojunctions that encourage hole electron recombination.

Pure titanium dioxide and related materials are well known for their abilities to activate, with near-UV radiation, many chemical reactions at temperatures for which the thermally activated processes proceed at negligible rates.[1–3] The introduction of iron as well dispersed Fe^{3+} ions into the TiO_2 structure has been shown to favour the reductive photofixation of dinitrogen to ammonia in the presence of adsorbed water in the form of hydroxyl ions.[4–6] In Part 1[7] of this study, structural and magnetic investigations of the progressive effects of increasing the nominal concentration of Fe^{3+} from 0.5 to 10 atom%, and the firing temperatures, have shown that the solid-state chemistry is complex, particularly at the higher concentrations of Fe^{3+} and at the higher firing temperatures. The complexities are related to the following aspects: (I) the phase transition from anatase (A) to rutile (R) which, in the pure material, becomes significant only at temperatures in the region of 973 K; (II) the apparent existence of solubility limits for the dispersed form of Fe^{3+} in these phases; (III) the precipitation of an iron oxide phase in the more concentrated systems; and (IV) the conversion of iron(III) oxide into pseudo-brookite (PB) by interaction with the TiO_2 structure at elevated temperatures.[8]

Separate studies of these materials have revealed that only the more dilute systems exhibit any significant photoactivity[6] and then only after they have been treated at the lowest firing temperatures, namely 773 and 923 K. Since the effectiveness of these materials as photocatalysts is related to their ability to absorb photons, the entire range of specimens has been subjected to examination by surface-sensitive methods: DRS, XPS, scanning electron microscopy (SEM) and surface area determination by the physical adsorption of argon at 77 K. The principal objective of this examination is an attempt to correlate the surface properties of these solids with their photocatalytic properties for reduction of dinitrogen to ammonia.

† Part 1: ref. 7.

Experimental

The materials and the preparative methods which have been used in this study were described in detail in Part 1[7] together with a coding, *e.g.* TF/CP/1/773, which identifies the method of preparation, the nominal iron content (atom%) and the temperature in K at which the material has been fired in air for 24 h. Effective iron contents for the majority of the specimens were obtained from analyses by Mikroanalytisches Labor Pascher, Germany.

DRS

DR spectra in air at 300 K, in the wavelength range 380–700 nm were obtained using a Macbeth MS 2000 instrument with $BaSO_4$(s) as the reference material.

Surface Area Measurements

The surface areas of the powdered materials were determined by the adsorption of argon at 77 K, using a dynamic

method.[9] By performing the consecutive measurements of two adsorption isotherms at 77 K, with an intervening period of outgassing of 1 h, also at 77 K, an assessment of the relative porosities of the specimens was obtained from the differences in the corresponding adsorption isotherms.

XPS

XPS of C 1s, O 1s, Ti 2p and Fe 2p levels were recorded on a Leybold–Heraeus LHS-10 spectrometer operating with a pass energy of 50 eV. Al-Kα radiation was used as the excitation source and the spectra were stored on a Hewlett-Packard HP 1000E computer, linked directly with the spectrometer, by means of which the spectral data were processed for peak area estimation for the various levels after removal of the background signals using the method due to Shirley.[10] In order to estimate the atomic concentrations, and their relative abundances, instrumental sensitivity factors supplied with the spectrometer have been used. The values of these factors are very similar to those reported elsewhere[11] and the binding energy (E_b) reference has been taken at the Ti $2p_{3/2}$ level at 458.5 eV. The spectra were recorded on lightly pressed pellets mounted in a port-hole specimen holder and in these conditions a single small C 1s peak due to adventitious elemental carbon on the specimens was observed at 284.6 eV. Sputtering of the specimen surfaces was carried out in the preparation chamber of the spectrometer with a Penning ion source using argon at an accelerating voltage of 3.5 kV. Under these conditions a calibration with a Ta_2O_5 standard gave an etching rate of *ca.* 1.2 nm min^{-1}.

SEM

SEM measurements were performed using a Phillips microscope, model 505, operating at 25 kV on specimens upon which a thin layer of gold had been evaporated. An electron microprobe used in an energy-dispersive mode (EDX) was employed to obtain quantitative information on the distribution of iron in the specimens.

Results and Discussion

DRS

(a) Pure Titanium Dioxide

Since titanium dioxide is the matrix in which the Fe^{3+} ions have been dispersed, it was necessary to make measurements on the various pure titania preparations into which the Fe^{3+} has been inserted; namely the solid precipitated from a $TiCl_3$ solution by ammonia (TiO_2[hp]), Degussa P25 (TiO_2[Dg]), and Tioxide CL/DD/1628/2 (TiO_2[TOx]). Significant differences in the crystal structures of these preparations have been reported elsewhere,[7,12–14] and these differences in structure, together with effects of variation in particle size, can be seen in the reflectance spectra[15] and in Fig. 1A. The specimen, TiO_2 (hp), has an initial specific surface area of 38.5 m^2 g^{-1} and the reflectance spectrum is similar to the well known spectrum of anatase, although XRD analysis reveals a minor content of rutile. On heating the sample at 1073 and 1273 K, the specimens exhibit the reflectance spectrum of the rutile phase which is consistent with the anatase–rutile transition having occurred, accompanied by a substantial decrease in the surface area to *ca.* 1 m^2 g^{-1} due to sintering.

TiO_2 (Dg), as received, with a specific surface area of 44 m^2 g^{-1}, has been shown to be a mixture of the two phases, anatase and rutile, in the proportions 80 : 20. The reflectance spectrum is intermediate between those of pure anatase and of pure rutile, but the spectrum is closer to that of rutile than the corresponding physical mixture of the two phases in the same proportions. This characteristic raises the question of the relative positions of the crystalline phases in the particles of this particular preparation, a matter which has been addressed elsewhere.[14]

TiO_2 (TOx), as received, with a specific surface area of 1.9 m^2 g^{-1} has been shown by XRD to be predominantly rutile and the reflectance spectrum is consistent with this observation.

(b) Iron-doped Specimens

It is clear that the reflectance spectra of every specimen containing iron have increased absorbances in the range 400–650 nm (Fig. 1B–D). The impregnated specimens, TF/Dg and TF/TOx, possess higher absorbances at the lower firing temperatures due to the accumulation of iron-rich layers at the surfaces, the surface accumulation being greatest for the TOx specimens (lowest specific areas) for any particular nominal concentration of iron. At the highest temperature (1273 K), the differences in the corresponding spectra are smaller, but the absorbances are in general larger than at the lower firing temperatures.

(i) 0.5 *atom*% Fe^{3+}(773–1273K); Fig. 1B. At 773 K, the relative order of the spectra for the three different preparative methods is consistent with the TF/CP solid having the lowest surface concentration of iron, with the other specimens, TF/Dg and TF/TOx, showing increased absorbances due to iron-rich surface layers. At 923 K, the TF/CP and TF/Dg specimens show little difference from the spectra obtained for these specimens fired at 773 K, but the TF/TOx specimen acquires a small but detectable enhancement in absorbance in the region 450–550 nm.

(ii) 1 *atom*% Fe^{3+} (773–1273 K); Fig. 1C. At 773 K, the spectra remain in the same relative order as for those containing 0.5 atom% Fe^{3+}, but the corresponding spectra show increased absorbances in the 400–650 nm range due to increasing surface concentrations of iron. At 923 K, the TF/CP and TF/Dg specimens yield similar spectra, whereas the TF/TOx specimen shows markedly enhanced absorbance in the range 400–550 nm relative to the other preparations and to the corresponding specimen containing 0.5 atom% of iron. At 1273 K, each specimen absorbs strongly in the range 400–550 nm, there being only marginal differences between them.

(iii) 5 *atom*% Fe^{3+} (773–1273 K); Fig. 1D. At 773 K, the spectra are very similar, with strong absorbances throughout the wavelength range 400–650 nm. At 923 K, differences between the spectra become apparent, and in the case of the TF/CP and TF/Dg specimens, decreases in absorbances are observed in comparison with the corresponding solids at 773 K, but for the TF/CP specimen this relative change is smaller; the TF/TOx spectra, however, do not change much as a result of the increased firing temperature. At 1273 K, the spectra of the TF/CP and TF/Dg specimens are almost identical, but the absorbance of the TF/Dg specimen has increased significantly from the spectrum of that solid fired at 923 K, whereas the TF/CP spectrum has remained unchanged. Most significantly there is a strong enhancement in the absorbance of the TF/TOx specimen in the wavelength range 500–650 nm.

XPS

Fig. 2 shows the variations in intensity and in shape of the O 1s spectra arising from the calcination of TiO_2 specimens containing 2 and 5 atom% of iron.

Fig. 3 shows the variation in the intensity and in the shapes of the Fe 2p peaks as the lattice is progressively

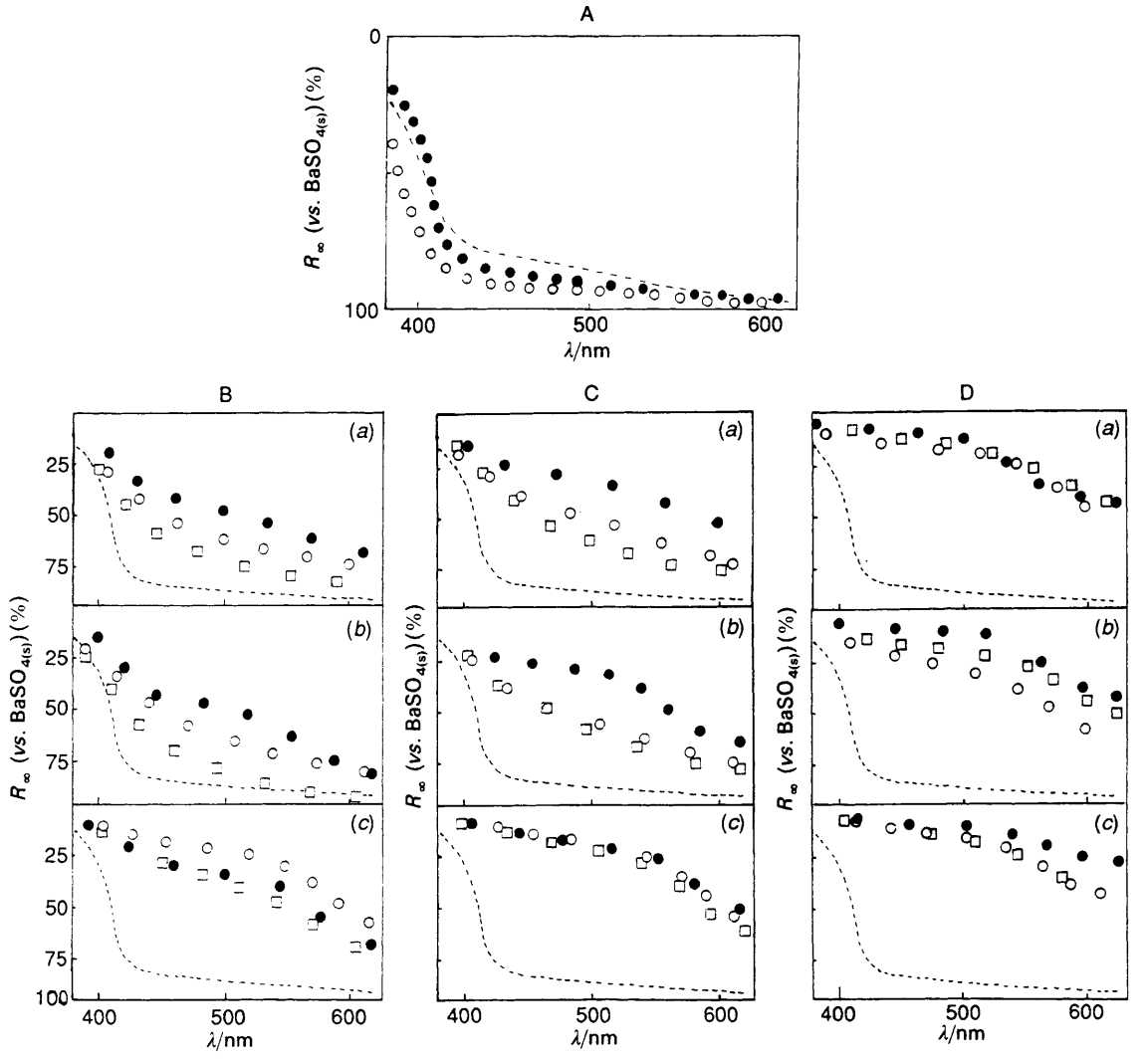

Fig. 1 A, DR spectra of the TiO_2 preparations at 300 K upon which the Fe^{3+}/TiO_2 systems are based: ●, rutile (TOx); (– – –) TiO_2(hp); ○, TiO_2(Dg). B, DR spectra of Fe^{3+}/TiO_2 powders (0.5 atom% Fe^{3+}) at 300 K following calcination in air at various temperatures for 24 h: ○, TF/Dg series; ●, TF/TOx series; □, TF/CP series; (– – –) rutile (TOx). (*a*) 773 K, (*b*) 923 K, (*c*) 1273 K. C, DR spectra of Fe^{3+}/TiO_2 powders (1 atom% Fe^{3+}) at 300 K following calcination in air at various temperatures for 24 h: ○, TF/Dg series; ●, TF/TOx series; □, TF/CP series; (– – –) rutile (TOx). (*a*) 773 K, (*b*) 923 K, (*c*) 1273 K. D, DR spectra of Fe^{3+}/TiO_2 powders (5 atom% Fe^{3+}) at 300 K following calcination in air at various temperatures for 24 h: ○, TF/Dg series; ●, TF/TOx series; □, TF/CP series; (– – –) rutile (TOx). (*a*) 773 K, (*b*) 923 K, (*c*) 1273 K.

loaded with larger quantities of iron at a fixed calcination temperature (773 K).

Fig. 4 shows a plot of the calculated Fe : Ti surface atomic ratios for the different TF/CP specimens as a function of the firing temperature. These ratios have been obtained by dividing the areas of the Fe 2p and Ti 2p peaks by their sensitivity factors, and correspond to the actual ratio of atoms detected by the electron energy analyser of the spectrometer. The results for the samples with contents of 0.5 and 5 atom% Fe^{3+}, indicate that heating up to 773 K produces decreases in the number of iron species present in the surface layers of the respective solids, which can be interpreted as being due to the incorporation of Fe^{3+} ions into the TiO_2 lattice with the consequent removal of Fe^{3+} ions from the surface layers by diffusion. These observations are consistent with those resulting from diffuse reflectance spectroscopy. For higher heating temperatures the Fe : Ti ratio increases for each specimen, suggesting a segregation of iron(III) species to the surface at all temperatures above 773 K. Discontinuities in the gradients of the graphs between 923 and 1073 K are probably related to the phase transition from anatase to rutile in these preparations. In relation to this phenomenon, it is noteworthy that the O 1s peaks in the spectra of each of the samples which have been heated at 1273 K show changes in their shapes suggesting that a greater heterogeneity has arisen in the surface oxide species due to the formation of iron-rich surface layers containing Fe_2TiO_5 and Fe_2O_3 in addition to the solid solution of Fe^{3+} in TiO_2, and XRD evidence[8] provides complementary support of this occurring. The most interesting specimens from the photocatalytic standpoint are those which are entirely solid solutions with distributions of iron in their surface layers which do not exceed the limit of solubility and which have been heated only at the lower temperatures (773 and 923 K) whereby a gradient of iron concentration exists from the surface towards the interior of the crystallites due to the relative slowness of the bulk diffusion process at these temperatures. These specimens have been investigated in more detail and a plot of the Fe : Ti surface atomic ratios as a function of the nominal iron content is shown in Fig. 5, in which there is an approximately linear relationship between these parameters up to an iron loading of 2 atom%. Specimens with a loading of 5 atom% show a marked deviation towards lower values than is predicted by the linear relationship. This deviation is explicable by the formation of iron-rich surface aggregates (*e.g.* TF/CP/5/773), some of which are of sufficient dimensions as to

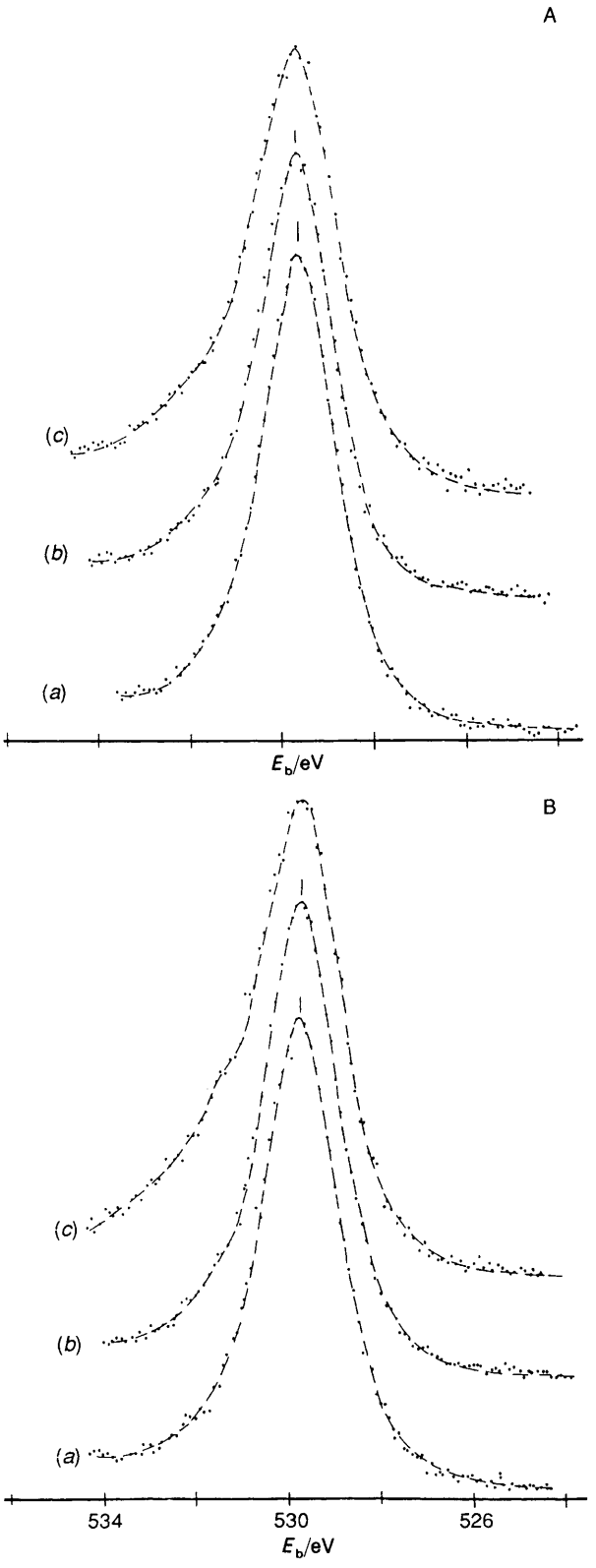

Fig. 2 Variations of the O 1s XP spectra of Fe^{3+}/TiO_2 specimens containing A 2 atom% and B 5 atom% of Fe as a function of the calcination temperature: (*a*) 923, (*b*) 1073 and (*c*) 1273 K

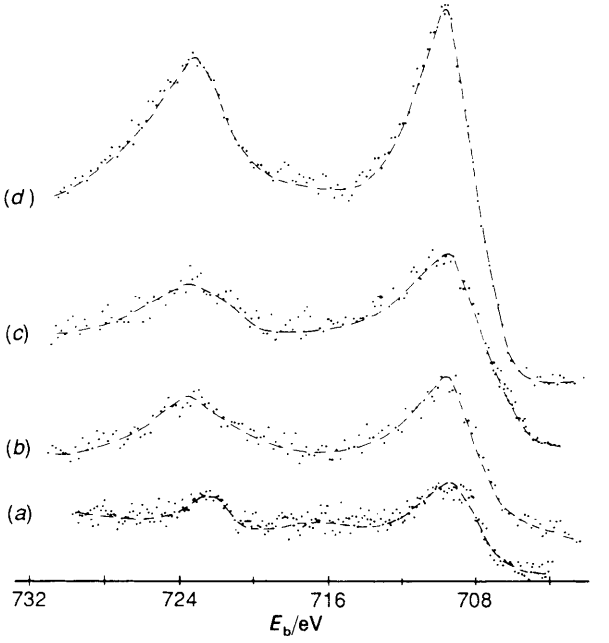

Fig. 3 Variations of the Fe 2p XP spectra of Fe^{3+}/TiO_2 specimens as a function of the nominal iron content following calcination at 773 K: (*a*) 0.5%, (*b*) 1%, (*c*) 2% and (*d*) 5%

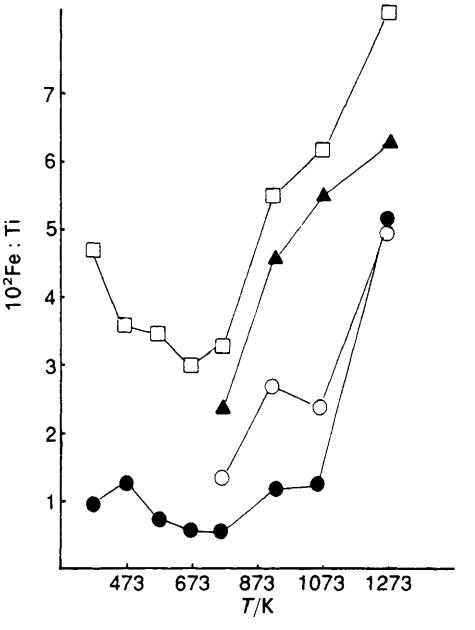

Fig. 4 Variation of the Fe : Ti surface atomic ratio in TF/CP specimens as a function of the calcination temperature in air: ●, TF/CP/0.5; ○, TF/CP1; ▲, TF/CP/2; □, TF/CP/5

exceed the escape depth (λ) of the photoelectrons, leading to a lowering of the intensity of the iron signals. Enrichment of iron at the surface of TF/CP/5/773 is also revealed by the sputtering profiles presented in Fig. 6. According to a model presented elsewhere[16] to describe the sputtering behaviour of particulate materials, the initial decrease in the Fe : Ti atom ratio when the specimen is subjected to sputtering, and which is not observed in the corresponding specimens TF/CP/0.5/923 and TF/CP/1/923, probably indicates the existence of very small particles of Fe_2O_3 or an enrichment of iron in the top-most layers of the surface. The flat profiles obtained with TF/CP/0.5/923 and TF/CP/1/923 are consistent with there being more uniform distributions of Fe^{3+} in the surface layers. From further inspections of Fig. 5 and 6, it is suggested that the distribution of Fe^{3+} species may not be completely uniform within the particles (*i.e.* inhomogeneous solid solution), there being an enrichment of the surface layers to a depth of *ca.* 20–40 nm as estimated from the sputtering rate measurement. For a completely homogeneous distribution of iron species, the values of the Fe : Ti surface atomic ratios should conform to the dotted line shown in Fig. 5. Note that

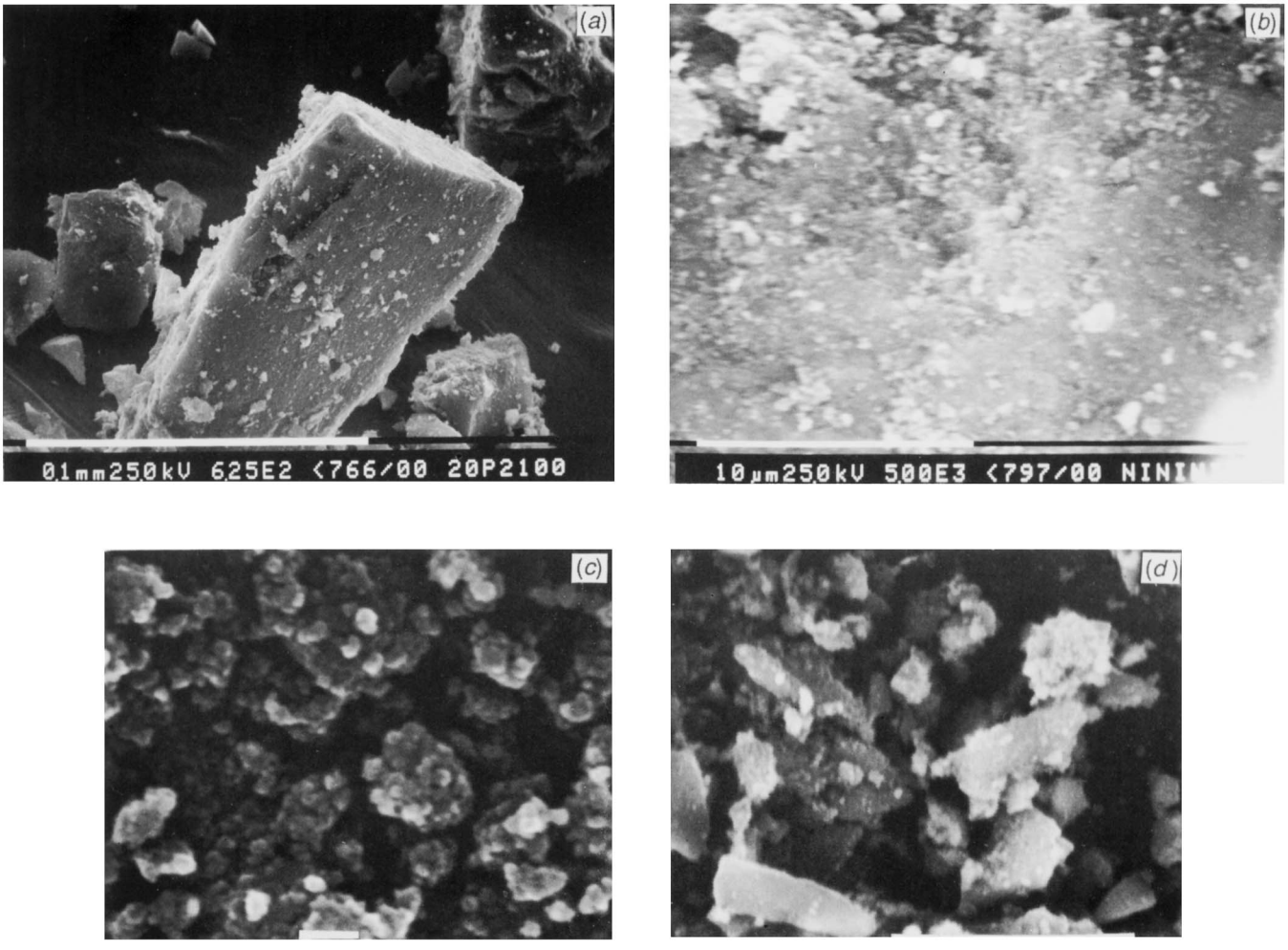

Plate 1 Scanning electron micrographs of precursor TiO_2 (*a*) and a series (*b*), (*c*) and (*d*) of Fe^{3+}/TiO_2 specimens: (*a*) TiO_2(hp) (×625) (bar scale = 100 μm), (*b*) TF/CP/0.5/773 (×5000) (bar scale = 10 μm), (*c*) TF/CP/1/773 (×10000) (bar scale = 1 μm), (*d*) TF/CP/2/773 (×4400) (bar scale = 10 μm)

R. I. Bickley *et al.* (*Facing p.* 2261)

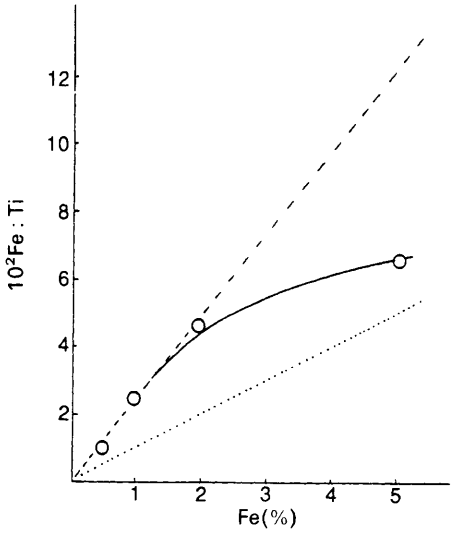

Fig. 5 Fe : Ti surface atomic ratio as a function of the nominal iron content of the TF/CP series of Fe^{3+}/TiO_2 preparations. (····) Predicted for a homogeneous solid solution.

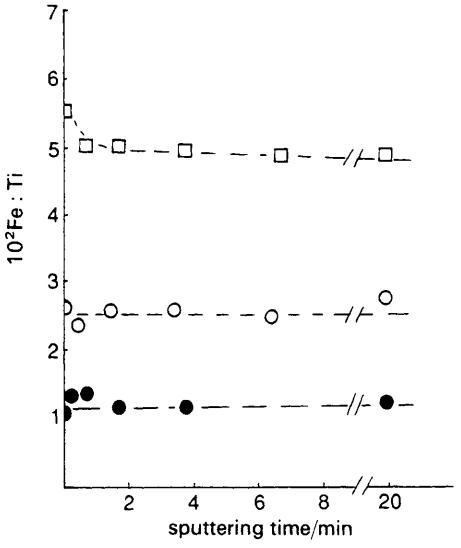

Fig. 6 Effect of sputtering on the Fe : Ti surface atomic ratio: ●, TF/CP/0.5; ○, TF/CP1; □, TF/CP/5

the Fe : Ti atomic ratio decreases by about a factor of two as each coprecipitated precursor material is calcined at 773 K and that these ratios attain approximately the values expected from the nominal iron compositions (Fig. 4). Since the escape depths (λ) of the Fe 2p photoelectrons through Fe_2O_3 and through TiO_2 are similar,[17] it may be expected that photoelectrons escaping from similar depths in either of these substances will be attenuated similarly. Thus, the XPS data show that specimens containing up to about 2 atom% Fe^{3+} have it well distributed in the external layers of the particles in which the particle diameter (d) is less than or equal to λ Fe 2p, the escape depth. Note, however, that in these experiments *ca.* 20–40 nm average depth has been removed by sputtering but that, owing to the existence of a distribution of particle sizes, the constancy of the Fe : Ti atomic ratio may be due partly to the convolution of contributions from signals arising from a range of particle sizes. However, for TF/CP/5/773 the formation of iron-rich particles of different sizes, some of which are larger in diameter than the escape depth of the Fe 2p photoelectrons, on the surfaces of the iron-saturated TiO_2 grains, would explain that the Fe : Ti ratio obtained is smaller than expected on the basis of extrapolation of the ratio data from the nominal concentrations of iron (Fig. 5). Note also that each of the ratios is actually larger than would have arisen from uniform distributions of iron throughout the volume of the particles.

SEM

Plate 1 shows scanning electron micrographs of the precursor form of TiO_2 (TiO_2-hp) from which the iron-containing specimens are derived and a series of specimens which contain progressively increasing nominal amounts of iron which form the series TF/CP/0.5, TF/CP/1 and TF/CP/2/773. Crystallites of the precursor TiO_2 appear to have particle sizes ranging downwards from an upper size limit of *ca.* 100 μm with minute debris ($d \leqslant 1.5$ μm) adhering to the faces of the larger crystallites. However, the co-precipitated iron-containing solids, TF/CP/1 and TF/CP/2, are composed of much smaller particles, the largest of which are aggregates of particles in the size range, $\lesssim$0.1–0.2 μm in TF/CP/1, whilst they are rather larger in TF/CP/2 where some surface debris is again apparent. In TF/CP/0.5 the morphology is less clear but the presence of many small particles is again evident without there being any of the larger aggregate sizes that occur in TF/CP/1 and TF/CP/2.

Most significantly, the EDX analyses for iron give variable amounts consistent with the iron being non-uniformly distributed, particularly in the impregnated specimens where it is considered that concentrated solutions of iron nitrate are formed during the initial evaporation process mainly in inter-particulate interstices, which result in high local concentrations of iron(III) oxide following the thermal decomposition of the iron(III) nitrate at elevated temperatures ($T \geqslant 773$ K). Whereas in the TF/CP specimens the EDX analyses were variable ($\pm$10%), the mean values were not substantially different from the nominal contents of iron, the corresponding analyses for the impregnated specimens were significantly larger than the nominal assignments and showed much greater degrees of variability; *e.g.* TF/TOx/2/773 showed a mean iron content of 3.2 $\pm$ 1.1 atom% which indicates that calcination in air for 24 h at 773 K is insufficient to enable the iron species to diffuse completely into the TiO_2 lattice with the consequence that such specimens have been quenched in a non-equilibrium condition in which gradients of iron concentration must exist within the particles. Clearly these results are compatible with the XPS observations.

Discussion

In Part 1,[7] magnetic susceptibility measurements revealed the presence of an antiferromagnetic phase, after firing in air at 923 K solids which contained in excess of *ca.* 3 atom% of Fe^{3+} in the TiO_2 matrix. This characteristic was ascribed to the precipitation of α-Fe_2O_3 on the surfaces of the crystallites. At higher firing temperatures it was found that the α-Fe_2O_3 phase would react with the iron-saturated TiO_2 matrix (1073 and 1273 K) to produce Fe_2TiO_5 (PB). The current surface study provides evidence which is compatible with the information reported in Part 1.[7] The DRS and XPS studies show collectively that enrichment of the surfaces of the solids by iron species commences at temperatures as low as 773 K, although no evidence of the existence of a new bulk phase was detectable at 773 K in the previous study[7] by X-ray diffraction. Also it has not been possible to identify the presence of α-Fe_2O_3 or Fe_2TiO_5 from the Fe 2p, Ti 2p and O 1s signals. However, changes in the bandshapes as a function of the calcination temperature suggest that new surface phases are being formed at the more elevated temperatures at

which α-Fe_2O_3 and/or Fe_2TiO_5 are detectable in the XRD powder diffraction patterns.[7,8]

It is now clear that the low-temperature surface enrichment of these solids with an iron-rich phase is consistent with there being a form of solubility limit, which results in a poorly ordered or amorphous iron-oxide phase at 773 K possessing no antiferromagnetic activity but which crystallises at 923 K into magnetically well ordered α-Fe_2O_3. Accompanying the crystallisation of the amorphous phase is its transformation into crystallites of sufficient sizes to exceed the escape depth (λ) of the Fe 2p photoelectrons while the adjacent TiO_2 matrix contains a saturated solution of Fe^{3+} ions. The overall situation is depicted in Fig. 7, which accounts also for the very variable analyses for iron obtained by EDX measurements from the solids with higher nominal concentrations of iron. Complementary evidence in support of this conclusion has emerged recently from a similar study of Fe^3/TiO_2 specimens produced by the impregnation method[18] in which a large degree of variability in the distribution of iron species has been reported, including evidence to suggest that microcrystallites of pure TiO_2 can be identified on the surfaces of the larger iron-containing crystallites. These authors also report evidence for the segregation of iron oxide at 773 K from infrared spectroscopy, where vibrational bands at 450–460 cm^{-1} have been ascribed to α-Fe_2O_3.

Photocatalytically only those specimens which contain Fe^{3+} ions that are well dispersed as a solid solution in the TiO_2 matrix show any significant activity for the photocatalytic reduction of dinitrogen to ammonia.[5] In the current study, such systems are typically only those which contain $\leqslant 1$ atom% of Fe^{3+}; *i.e.* those which are well removed from the saturation condition or from conditions in which the precipitation of an iron oxide phase can occur. In the DRS study, these specimens show some enhancement in absorbance on the low-energy side of the absorption edge of the TiO_2 matrix at 410 nm (Fig. 1B–D), suggesting the existence of a range of electronic states ($\Delta E \approx 1$ eV) between the conduction band and the valence band of the host TiO_2 matrix ($E_g \approx 3$ eV). Since these solids display the anatase or the rutile unit-cell configuration, albeit possibly modified by the coexistence of Fe^{3+} centres on titanium(IV) lattice positions and vacant oxygen lattice positions to compensate for the charge deficiency on the cation sub-lattice, they will effectively act as heavily doped forms of TiO_2. Such solids will display optical transitions from valence band to conduction band as occurs in undoped TiO_2, or transitions of lower energies involving the interband states introduced by doping. As such, the minimal photocatalytic activity of the host matrix in dinitrogen fixation may be modified by the existence of the inter-band states and by the corresponding adjustment to the position of the Fermi level of these solids. Additionally, the presence of surface iron(III) species and of vacant oxygen sites may modify the thermally activated interactions of dinitrogen and of water with these solids. Some evidence, which has been interpreted in these terms, has been published recently[18] which shows that water adsorption displays a greater diversity of adsorption states on Fe^{3+}/TiO_2 systems containing $\leqslant 5$ atom% Fe^{3+} in comparison to pure TiO_2, without any major effect on the physisorption of dinitrogen.[19]

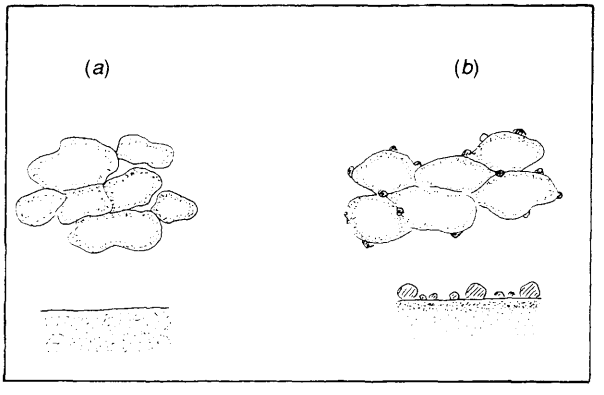

Fig. 7 Schematic diagram of Fe^{3+}/TiO_2 particles illustrating the formation of iron-rich surface crystallites: (*a*) poorly ordered material, (*b*) particles containing iron-rich surface crystallites

A consequence of the existence of a greater diversity of adsorption states of water on the Fe^{3+}/TiO_2 surfaces than has been found to exist on pure TiO_2 surfaces relates to the roles played by those adsorbed states of water in the photocatalytic process. It is well established that the adsorbed states of water on pure titania have a marked influence upon the photocatalytic activity in photo-oxidation processes;[20] the existence of such states, and of hydroxy groups in particular, appearing to be a prerequisite for the surfaces having appreciable activity for such reactions. Hydroxy groups, formed by the dissociative adsorption of molecular water, are considered to act as traps for the positive holes formed during the absorption of a photon of bandgap radiation, thereby releasing the electron which can be captured by the oxidising medium, which is frequently adsorbed molecular oxygen or its dissolved counterpart.

$$TiO_2 + h\nu(\geqslant E_g) \rightarrow (h_{vb}\text{–}e_{cb})$$

$$(h_{vb}\text{–}e_{cb}) + OH^-_{(ads)} \rightarrow {}^{\bullet}OH_{ads} + e^-_{cb}$$

$$e^-_{cb} + O_{2(ads)} \rightarrow O^-_{2(ads)}$$

Similar conditions appear likely to prevail in the photoreduction of dinitrogen with water vapour, in which the dissociation of water must be an early step. The fission of the molecular bond of dinitrogen probably arises from the attack upon it by hydrogen atoms which are created in a manner similar to the mechanism proposed for their creation on Pt^0/TiO_2 surfaces[21] for the photosplitting of water:

$$(h_{vb}\text{–}e_{cb}) + Pt^0_n \rightarrow h^+_{vb} + Pt^-_n$$

$$h^+_{vb} + H_2O_{(ads)} \rightarrow H^+_{(ads)} + {}^{\bullet}OH$$

$$H^+_{(ads)} + e^- \rightarrow H^{\bullet}_{(ads)}$$

$$H^{\bullet}_{(ads)} + H^{\bullet}_{(ads)} \rightarrow H_2(g)$$

In the case of the well crystallised Fe^{3+}/TiO_2 system, the electron trap is probably the Fe^{3+} centre which acts in a manner comparable to that suggested previously for finely dispersed platinum metal. Following the formation of adsorbed hydrogen atoms, these centres can interact with adsorbed molecular nitrogen to produce ammonia in a sequence of hydrogenation steps:[22,23]

$$H_{(ads)} + N_{2(ads)} \rightarrow NH_{(ads)} \xrightarrow{H} NH_{2(ads)} \xrightarrow{H} NH_{3(ads)} \rightarrow NH_{3(g)}$$

In contrast to the well dispersed dilute solid solutions of iron(III) in TiO_2 ($[Fe^{3+}] \leqslant 1\%$) the more concentrated systems do not display any photocatalytic activity. They consist of iron-saturated TiO_2 matrices which form cores for amorphous iron-rich surfaces phases, or act as supports for well crystallised grains of iron(III) oxide and for patches, or islands, of Fe_2TiO_5. The DRS data show intense absorption of electromagnetic radiation ranging from the absorption edge of the host matrix (TiO_2) at 410 nm through to beyond 650 nm (Fig. 1D). While it has not been established that the iron-saturated solid solution alone is photoinactive and it is quite possible that its behaviour would be compatible with

the more dilute systems, the co-existence of distinct phases does appear to deactivate the system for photocatalysis. Two factors can be identified which may contribute to the process of photocatalyst deactivation. The first is a simple optical screening effect in which the iron oxide surface phase absorbs all of the electromagnetic radiation and the core phase either cannot be activated directly, or alternatively the contact between the two phases creates an electronic heterojunction because of the differing values of their individual Fermi levels. Since specimens which contain the well crystallised α-Fe_2O_3 are also photoinactive, and that in such specimens the iron-saturated TiO_2 matrix need not be necessarily covered entirely by iron(III) oxide, or by Fe_2TiO_5, then the screening effect may operate over a proportion of the external surface, but activation of the remaining portion of the iron-saturated surface is possible. In this situation it would appear that the heterojunction formed by the contact between two chemically distinct phases must play an important role in rendering these materials inactive in the reductive photo-fixation of dinitrogen by promoting hole–electron recombination through favourable juxtaposition of the respective conduction and valence bands. For well crystallised Fe^{3+}/TiO_2 and α-Fe_2O_3, the band diagrams can produce two possibilities for the heterojunction based upon existing published data[24–26] (Fig. 8), namely conditions arising from contact between a heavily doped TiO_2 matrix and a non-stoichiometric iron(III) phase, Fig. 8(*b*), which would facilitate

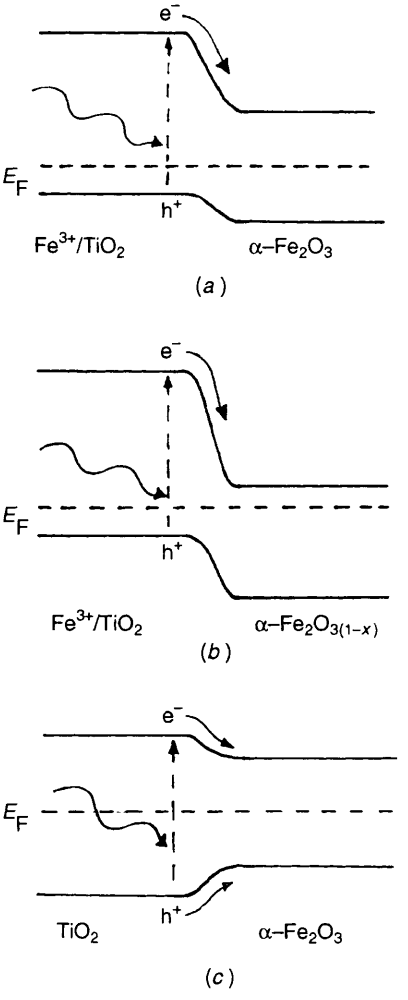

Fig. 8 Heterojunctions created by contact between dissimilar phases: (*a*) Fe^{3+}/TiO_2 in contact with pure α-Fe_2O_3, (*b*) Fe^{3+}/TiO_2 in contact with non-stoichiometric Fe_2O_3, (*c*) TiO_2 in contact with α-Fe_2O_3

electron transfer from the Fe/TiO_2 phase to the iron oxide while presenting hole transfer with an activation energy of *ca.* 35–40 kJ mol^{-1}. In circumstances in which the α-Fe_2O_3 phase has crystallised into a stoichiometric well ordered, antiferromagnetic condition, similar circumstances prevail for the conduction-band electrons, but the magnitude of the activation energy for hole transport into the iron oxide phase has been reduced to $\leqslant 10$ kJ mol^{-1} with hole–electron recombination in the α-Fe_2O_3 phase now more favoured, Fig. 8(*a*). Finally, it should be recognized that whereas band structures can form an acceptable basis for interpreting the behaviour of well defined crystal lattices, the situation, which has been shown to exist at 773 K for the more heavily loaded specimens, presents the possibility of contact between an amorphous overlayer of iron(III) oxide and a well crystallized saturated solution of Fe^{3+} in TiO_2. The existence of Anderson states has been proposed elsewhere[20] for poorly crystallized solids, and for one of the forms of pure TiO_2 (Degussa, P25)[14] used in the present study. Accordingly one may expect similar conditions to prevail in the amorphous overlayer of iron(III) oxide which forms at 773 K when the progressive anatase-to-rutile phase transition occurs. This transition is assisted by the presence of anion vacancy-creating Fe^{3+} ions, which results in the precipitation of the iron-rich oxide layer as a consequence of the rutile phase having a lower limit of solubility[12] for Fe^{3+} than the anatase phase. Since the observed effect of the overlayer is to cause deactivation, it is assumed that the existence of Anderson states in the amorphous overlayer will promote a favourable condition for hole–electron recombination. In the absence of spectral data for pure Fe_2TiO_5, one is led to conclude that its presence in the overlayers of those specimens that have been calcined at the highest temperatures produces a deactivation of the photocatalytic process for similar reasons to those that have been suggested for the specimens containing well crystallised α-Fe_2O_3 overlayers.

The authors thank the British Council, the Ministero dell'Università e della Ricerca Scientifica e Tecnologica (MURST), Italy and the Consejo Superior de Investigaciones Cientificas (C.S.I.C.) in Sevilla and Madrid, Spain for financial support and the provision of facilities.

References

1 M. A. Fox, in *Photocatalysis and Environment, NATO ASI Series C*, ed. M. Schiavello, Kluwer, Dordrecht, 1988, vol. 237, pp. 445–467.
2 K. J. Green and R. Rudham, *J. Chem. Soc., Faraday Trans.*, 1993, **85**, 1867.
3 F. Sabin, T. Türk and A. Vogler, *J. Photochem. Photobiol. A, Chem.*, 1992, **63**, 99.
4 G. N. Schrauzer and T. D. Guth, *J. Am. Chem. Soc.*, 1977, **99**, 7189.
5 V. Augugliaro, F. D'Alba, L. Rizzuti, M. Schiavello and A. Sclafani, *Int. J. Hydrogen Energy*, 1982, **7**, 851.
6 J. Soria, J. C. Conesa, V. Augugliaro, L. Palmisano, M. Schiavello and A. Sclafani, *J. Phys. Chem.*, 1991, **95**, 274.
7 R. I. Bickley, J. S. Lees, R. J. D. Tilley, L. Palmisano and M. Schiavello, *J. Chem. Soc., Faraday Trans.*, 1992, **88**, 377.
8 R. I. Bickley, T. Gonzalez-Carreno and L. Palmisano, *J. Mat. Chem. Phys.*, 1991, **29**, 475.
9 H. Bosch and E. Peppelenbos, *J. Phys. E*, 1977, **10**, 605.
10 D. A. Shirley, *Phys. Rev. B*, 1972, **5**, 4709.
11 C. D. Wagner, L. E. Davies, M. U. Zeller, J. A. Taylor, R. H. Raymond and L. E. Gale, *Surf. Interface Anal.*, 1979, **1**, 26.
12 D. Cordischi, N. Burriesci, F. D'Alba, M. Petrera, G. Polizzotti and M. Schiavello, *J. Solid State Chem.*, 1985, **56**, 182.
13 R. I. Bickley, T. Gonzalez-Carreno, J. S. Lees, L. Palmisano and R. J. D. Tilley, *Proc. 8th Int. Conf. on the Photochemical Conversion and Storage of Solar Energy*, IPS8 Alba Photograf., Palermo, Italy, 1990, p. 197.

14 R. I. Bickley, T. Gonzalez-Carreno, J. S. Lees, L. Palmisano and R. J. D. Tilley, *J. Solid State Chem.*, 1991, **92**, 178.
15 R. I. Bickley, T. Gonzalez-Carreno and L. Palmisano, in *Preparation of Catalysts IV*, ed. B. Delmon, P. Grange, P. A. Jacobs and G. Poncelet, Elsevier, Amsterdam, 1987, p. 297.
16 A. R. Gonzalez-Elipé, J. P. Espinos, A. Fernandez and G. Munuera, *J. Catal.*, 1991, **130**, 627.
17 M. P. Seah and W. A. Derich, *Surf. Interface Anal.*, 1979, **1**, 2.
18 J. A. Navio, M. Macias, M. Gonzalez-Catalan and A. Justo, *J. Mater. Sci.*, 1992, **27**, 3036.
19 A. B. Rives, T. S. Kulkarni and A. L. Schwaner, *Langmuir*, 1993, **9**, 192.
20 R. I. Bickley, G. Munuera and F. S. Stone, *J. Catal.*, 1973, **31**, 398.
21 M. Gratzel, *Photocatalysis and Environment, NATO ASI Ser., Ser. C*, 1988, **237**, 384.
22 S. Sato and J. M. White, *J. Am. Chem. Soc.*, 1980, **102**, 7206.
23 M. Schiavello, L. Rizzuti, R. I. Bickley, J. A. Navio and P. L. Yue, *Proc. 8th Int. Congr. Catal.* (Berlin) 1984, vol. 3, pp. 383–394.
24 B. Levy, in *Photochemical Conversion and Storage of Solar Energy*, ed. E. Pelizzetti and M. Schiavello, Kluwer, Dordrecht, 1991, pp. 337–392.
25 M. Grätzel, in *Photocatalysis and Environment, NATO ASI Series C*, 1988, vol. 237, p. 369.
26 G. A. Somorjai, in *Homogeneous and Heterogeneous Photocatalysis, NATO ASI Ser., Ser. C*, 1986, vol. 174, p. 469.

Paper 3/07545A; *Received* 23*rd December*, 1993